Solar Physics (2005) 226: 45–72

RESIK: A BENT CRYSTAL X-RAY SPECTROMETER FOR STUDIES OF SOLAR CORONAL PLASMA COMPOSITION

J. SYLWESTER[1], I. GAICKI[1], Z. KORDYLEWSKI[1], M. KOWALIŃSKI[1], S. NOWAK[1], S. PŁOCIENIAK[1], M. SIARKOWSKI[1], B. SYLWESTER[1], W. TRZEBIŃSKI[1], J. BĄKAŁA[1], J. L. CULHANE[2], M. WHYNDHAM[2], R. D. BENTLEY[2], P. R. GUTTRIDGE[2], K. J. H. PHILLIPS[3], J. LANG[4], C. M. BROWN[5], G. A. DOSCHEK[5], V. D. KUZNETSOV[6], V. N. ORAEVSKY[6], A. I. STEPANOV[6] and D. V. LISIN[6]

[1]*Space Research Centre, Polish Academy of Sciences, 51-622 Kopernika 11, Wrocław, Poland (e-mail: js@cbk.pan.wroc.pl)*

[2]*Mullard Space Science Laboratory, University College London, Holmbury St. Mary, Dorking, Surrey RH5 6NT, U.K.*

[3]*National Research Council Senior Research Associate, Code 682, NASA Goddard Space Flight Center, Greenbelt, MD 20771, U.S.A.*

[4]*Space Science and Technology Department, Rutherford Appleton Laboratory, Chilton, Didcot, Oxon OX11 0QX, U.K.*

[5]*E. O. Hulburt Center for Space Research, Code 7670, Naval Research Laboratory, Washington, DC 20375-5352, U.S.A.*

[6]*Institute of Terrestrial Magnetism and Radiowave Propagation (IZMIRAN), Troitsk, Moscow, Russia*

(Received 9 August 2004; accepted 28 October 2004)

Abstract. We describe the RESIK (REntgenovsky Spektrometr s Izognutymi Kristalami) instrument, consisting of two double-channel X-ray spectrometers, designed to observe solar active region and flare plasmas. RESIK is one of the instruments making up the scientific payload of the Russian *CORONAS-F* solar mission. The uncollimated spectrometer uses two silicon and two quartz bent crystals observing flare, active region and coronal spectra in four wavelength bands with a resolving power ($\lambda/\Delta\lambda$) of $\sim$1000. The wavelength coverage, 3.3 – 6.1 Å, includes emission lines of Si, S, Cl, Ar, and K and in the third diffraction order, the wavelength range includes He-like Fe lines (1.85 Å) and Ni lines (1.55 Å) with dielectronic satellites, emitted during intense, hot flares. The instrument is believed to be the best calibrated space-borne crystal spectrometer flown to date. The spectrometer dynamically adjusts the data gathering intervals from 1 s to 5 minutes, depending on the level of solar X-ray emission at the time of observation. The principal aims of RESIK are the measurements of relative and absolute element abundances in the emitting plasma and the temperature distribution of plasma (differential emission measure) over the temperature interval 3 and 50 MK. This paper summarizes the scientific objectives of RESIK and describes the design, characteristics, and performance of the instrument.

1. Introduction

Flares and active regions are observed in the corona as highly enhanced regions of soft X-ray emission, and are commonly believed to be powered by the release of energy stored in magnetic fields. Understanding the physical mechanisms behind this energy transformation represents one of the most challenging problems

of astrophysics. In the past 40 years, it has become clear that progress can best be made with the aid of observations in all parts of the electromagnetic spectrum. Spectrometers operating in the soft X-ray region provide valuable information about the temperature, ionization state, and any non-thermal and directed velocities of the emitting plasma. Among these are the scanning, flat crystal spectrometers on the early NASA *Orbiting Solar Observatories*, the U.S. Navy *P78-1* satellite, NASA's *Solar Maximum Mission* or *SMM* (the X-ray Polychromator/Flat Crystal Spectrometer), and the Japanese *Hinotori* spacecraft. Because of the length of time needed to scan particular portions of the X-ray spectrum, critical phases of flares were often missed with these spectrometers. Curved crystal spectrometers like the *SMM* Bent Crystal Spectrometer and the Bragg Crystal Spectrometer (BCS) on the Japanese *Yohkoh* spacecraft (Culhane *et al*., 1991) have an important advantage in this respect since they are designed to take complete spectra, generally over limited wavelength bands, over time intervals of only a few seconds. With strong emission lines like the resonance lines of highly ionized Ca and Fe, formed at high temperatures, spectral changes and thus information about physical conditions during the rapid development of particular flares can be followed (Antonucci, 1989).

The REntgenovsky Spektrometr s Izognutymi Kristalami (RESIK) bent crystal X-ray spectrometer on the Russian *CORONAS-F* solar spacecraft has been operating since spacecraft launch on 31 July 2001. Its wavelength coverage, 3.3–6.1 Å, has been very little explored by previous solar spacecraft. Spectra from solar flares seen by RESIK include strong emission lines of highly ionized Si, S, and Ar atoms, together with lines from the low-abundance, odd-Z elements K and Cl. Some of these lines are also seen in the spectra of bright, non-flaring active regions, and several lines have been observed for the first time in solar X-ray spectra. Brief descriptions of RESIK and initial observations are given by Sylwester *et al*. (2002, 2003), and Phillips *et al*. (2003). In this paper, we describe the *CORONAS-F* spacecraft (Section 2) and give more details about RESIK including its scientific objectives (Section 3), its concept, design and calibration (Section 4), and initial results (Section 5).

2. The CORONAS-F Spacecraft

The *CORONAS-F* spacecraft (Figure 1) is the second of two Russian space observatories devoted to solar and magnetospheric physics, designed to be operational during the 23rd solar cycle. Its primary objectives are the study of solar global oscillations, variations in the solar ultraviolet radiation, flare and active region X-ray, gamma-ray, and particle emission. Its launch, on 31 July 2001, followed the launch of the *Coronas-I* spacecraft in 1994 March which was intended to observe the Sun at solar minimum (Lebedev, Oraevsky, and Zhugzda, 1995). Among the 13 instruments on board *CORONAS-F* are the two soft X-ray high-resolution spectrometers

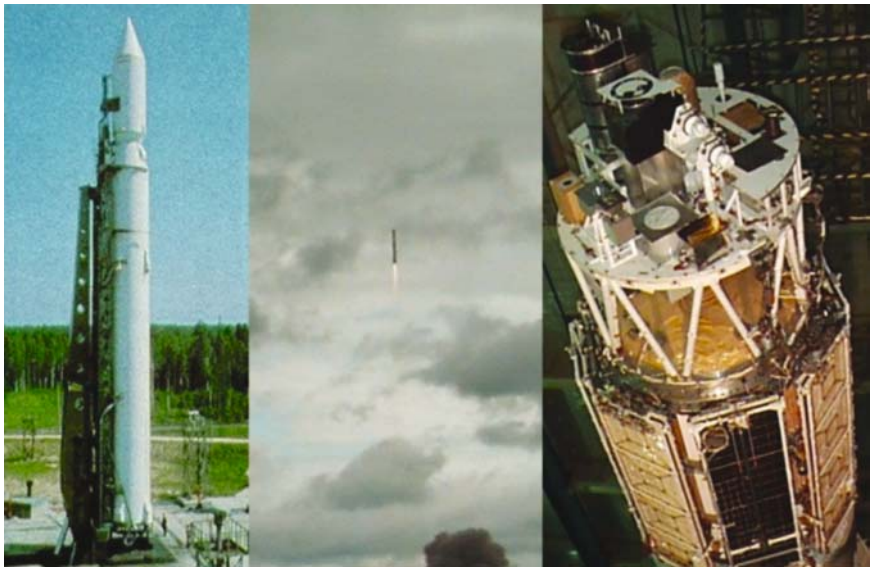

Figure 1. *Left*: The Cyclone SL-14 rocket on the launch pad at the Plesetsk Cosmodrome, northern Russia, on the morning of the launch, 31 July 2001. *Centre*: The cyclone rocket shortly after launch. *Right*: The instrument payload of *CORONAS-F*: the spacecraft is ∼1.5 m in diameter and weighs ∼2.5 tonnes. See Figure 3 for location of the RESIK instrument.

Diogeness and RESIK, built by teams led by the Space Research Centre, Polish Academy of Sciences, Wrocław, Poland. The Diogeness spectrometer uses scanning flat crystals to cover the wavelength ranges 2.83–3.36, 4.98–5.30, and 6.15–6.74 Å. The 11 Russian instruments, mostly built by groups at IZMIRAN (Troitsk), the Lebedev Physical Institute (FIAN) and other Russian Institutes include the RES-C spectropolarimeter, which obtains images of the Sun in X-ray emission lines due to He-like Fe (Fe XXV) and H-like Mg (Mg XII) as well as two XUV bands (around 200 and 300 Å); the Soft X-ray Telescope (SRT), which observes the Sun in narrow XUV bands centered on 171 Å (Fe IX, Fe X), 195 Å (Fe XII), 304 Å (He II) among others; the Solar Spectropolarimeter (SPR), observing polarization in 20–100 keV X-rays. These three instruments make up the so-called SPIRIT group. The remaining instruments are an X-ray Flare Spectrometer (IRIS), observing 2–200 keV flare X-rays, a hard X-ray and gamma-ray spectrometer (HELICON), observing in the energy range 10 keV–10 MeV; a Solar Ultraviolet Spectrophotometer (VUSS), observing the hydrogen Ly-α line at 1216 Å, Solar Cosmic Rays Complex (SKL) which comprises a cosmic ray monitor (MKL); and other monitoring instruments operating in the ultraviolet, X-rays and gamma-rays. The payload carries also instruments sensing the immediate particle environment. Further details about the instruments and data acquisition are given by Oraevsky and Sobelman (2002) and may be found on the web site *http://coronas.izmiran.rssi.ru/F/*.

The *CORONAS-F* spacecraft is in a near-circular orbit around the Earth with an altitude ranging from 501 to 549 km, and an orbital plane inclined at 82.5° to the equator; its orbital period is 94.9 min. The near-polar orbit allows periods of uninterrupted observation of the Sun for up to about 20 days: the longest satellite night lasts 35 min. Passages through the Earth's radiation belts require the X-ray instruments to be turned off; these include passages through the South Atlantic Anomaly (SAA) as well as the auroral oval (AO) regions near the magnetic poles. The spacecraft is controlled from the Flight Control Centre, Cosmic Information Technology Centre, IZMIRAN. Commands and uploads are sent daily from the tracking station at Neustrelitz, Germany. Updates can be received as little as 10 min before ground station contact. The operational lifetime of the satellite is expected to extend till 2007 when the spacecraft will enter the Earth's atmosphere. The satellite is stabilized such that its z-axis points to within 10 arc min of Sun centre with a roll stability of 3 arc sec s^{-1}. The roll angle may, however, assume any direction. Information about the roll angle for any given time, which is of importance for the RESIK instrument, is made available to the instrument groups by the SPIRIT team at the Lebedev Physical Institute. Figure 2 shows the time variations of the roll

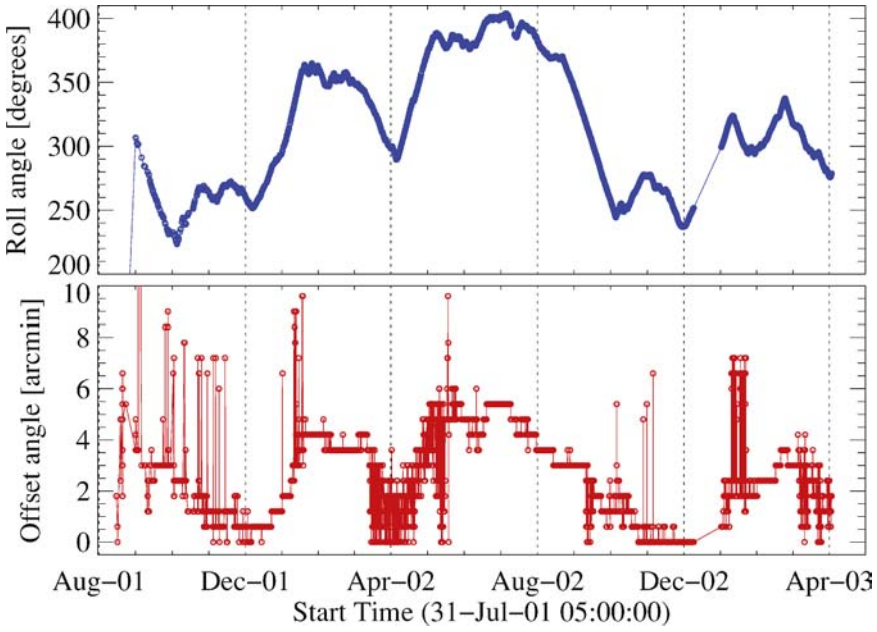

Figure 2. *Top panel*: Variations in the *CORONAS-F* spacecraft roll angle for the period 1 August 2001 – 30 April 2003. The rate of variations of the roll angle, which is a measure of the dispersion direction of the RESIK instrument, is never more than 1° per day. *Bottom panel*: Offset of the spacecraft z-axis measured from Sun centre for the same period of time (courtesy of SPIRIT Team, FIAN, Moscow).

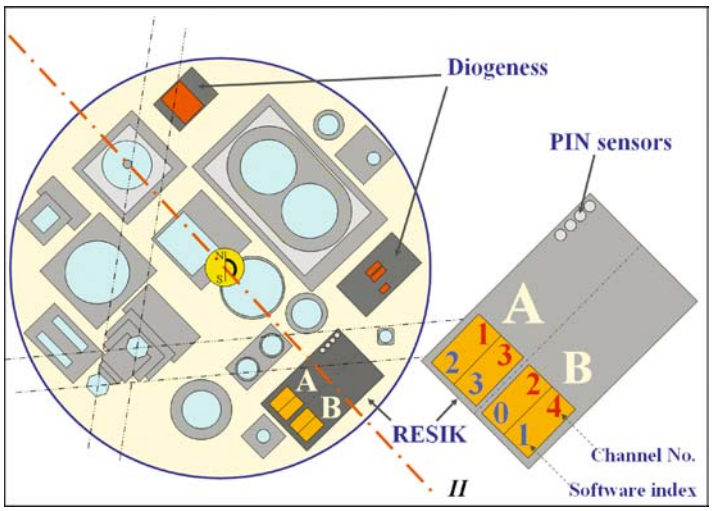

Figure 3. *Left*: Scheme of instruments' placement within the *CORONAS-F* payload as seen from the Sun. The main axis (*II*) is indicated together with roll angle readout convention. Darker shades indicate components of RESIK and Diogeness. *Right*: is an enlargement of the RESIK instrument, showing the disposition of spectrometers A and B and channel numbers (1 – 4), as used in the tables and figures here, and corresponding software indices (0 – 3) used in the instrument testing and preparation. Placement of the four radiation environment PIN sensors is also indicated.

angle and offset of the spacecraft z-axis from Sun center in the first 21 months of spacecraft operations.

The dispersion planes of both Polish spectrometers are co-aligned and perpendicular to the main spacecraft axis (line *II*, indicated in Figure 3). The position of this axis is indicated by arrow on each page of the RESIK catalogue (see Figure 6, upper right corner).

3. RESIK Scientific Objectives

The two primary scientific objectives of the RESIK instrument are to determine:

- the chemical composition of X-ray flare and active region plasmas using emission line and continuum intensities;
- the temperature structure of emitting regions based on the differential emission measure.

The differential emission measure (DEM) is defined here as $\phi(T_e) = N_e^2\, dT_e/dV$, where T_e and N_e are electron temperature and density, respectively, and V is the emitting volume.

The importance of the first objective has become evident in the past 10 years with the discovery that the abundances of elements in coronal active regions and flares are different from those in the photosphere depending on the value of the

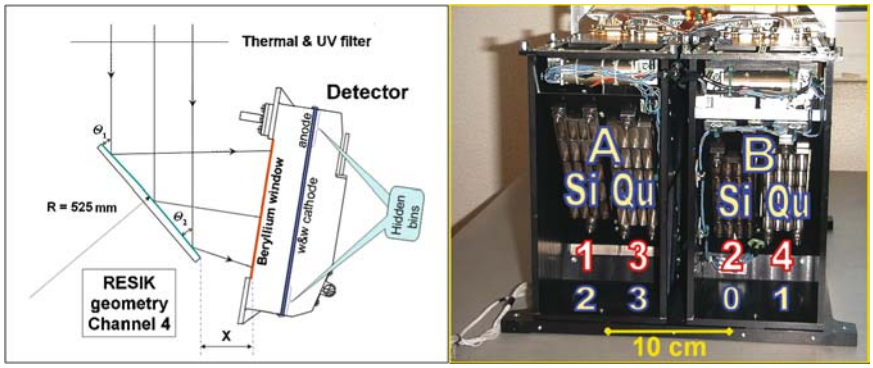

Figure 4. Left: Scheme of one of the four similar spectrometer sections making up the RESIK payload as seen from the side. The crystals are bent to cylindrical profiles (radius R is indicated), such that there is a slight change of incidence angle over the crystal surface ($\theta_1 > \theta_2$). The distance X indicated is the basic reference distance between the crystal edge and the edge of the detector Be window. *Right*: Annotated photograph showing the back side of the crystal supports with the disposition of spectrometers A and B, crystal material and channel numbers (1–4), assigned in order of wavelength and used in the tables and figures here. The corresponding software indices (numbers, 0–3) used for engineering purposes are shown for reference.

first ionization potential (FIP) of the element (Meyer, 1985; Feldman and Laming, 2000). Measurements from X-ray and extreme ultraviolet emission lines indicate that elements with FIPs $\lesssim$ 10 eV are more abundant in the corona than in the photosphere by factor of 3 or 4. Those with FIPs $>$ 10 eV have coronal abundances approximately equal to photospheric values (Feldman and Laming, 2000), though some observations suggest that they are less than photospheric by a factor of 2 (Fludra and Schmelz, 1999). It is possible that element abundances vary with time during flares (Sylwester, Lemen and Mewe, 1984) and also that the X-ray-emitting coronal plasmas of very short-lived, impulsive flares have photospheric abundances (Feldman and Laming, 2000).

The wavelength coverage of RESIK, 3.3–6.1 Å, is ideal for studying the abundances of a wide variety of elements with both low and high values of FIP. Tables II and III and Figure 13 show principal features identified as lines in spectra from a flare on 21 January 2003 (*GOES* class M1.9). (Channel numbers used here are those assigned in order of wavelength, though for software purposes an alternative scheme is used: see Figure 4.) Emission lines of Ar (FIP = 15.8 eV), S (FIP = 10.4 eV), and Si (FIP = 8.2 eV) are identifiable, some of which are very strong. Weaker line emission due to K, having the lowest FIP (4.3 eV) of any cosmically abundant element, and Cl (FIP = 13.0 eV) is also visible. Two of the channels (1 and 2) of RESIK observe continuum emission without appreciable instrumental contamination (due to fluorescence, see Section 4.7), so enabling absolute element abundances, i.e. with respect to hydrogen, to be determined. The instrument sensitivity is considered to be quite accurate, with an absolute accuracy better than

$\sim$15% (for discussion see Section 4.5). Therefore, it appears that fairly precise abundance determinations are possible.

The wavelength range of RESIK contains several lines whose relative intensities are temperature sensitive, so fulfilling the second objective. These include lines in the He-like Si (Si XII) sequence $1s^2-1snp$ ($n = 3, 4, 5$) and the intensities of any of these lines or their sum relative to the intensity of the $1s-3p$ (Lyβ) line of H-like Si depend on the ionization state of the plasma. All these lines are seen in channel 4 of RESIK. In addition, lines of He-like S (S XV), $1s^2-1snp$ ($n = 3$, 4, 5) are present in channel 3 spectra, the intensities of which are significantly different in their temperature dependence. A prominent feature of even small flares is the triplet of lines due to $1s^2-1s2l$ ($l = s$, p) of He-like Ar (Ar XVII) which, for a plasma in equilibrium, are also sensitive to T_e through the so-called G ratio (Pradhan, 1985). Another temperature-dependent line ratio is that of dielectronic satellites to the Si XIII $1s^2\,{}^1S_0-1s3p\,{}^1P_1$ line at 5.68 Å. RESIK observations indicate that the Si XII dielectronic satellite line at 5.82 Å, mostly due to $1s^2\,2p\,{}^2P_{3/2}-1s2p^3P3p\,{}^2D_{5/2}$ is strong relative to the 5.681 Å line during non-flaring periods, but weak otherwise, showing its temperature dependence (Sylwester *et al.*, 2003). These satellites appear to have been little used for application to solar flare spectra. Atomic data for their intensities (Chen, 1986; Dubau, 2004) have been used in a preliminary analysis of the temperature dependence of these lines (Phillips *et al.*, 2004).

In Figure 5, the emission functions characterizing the temperature dependence of photon flux at the spacecraft are plotted for the stronger lines seen by RESIK. The temperatures of maximum line emission are given in Tables II and III.

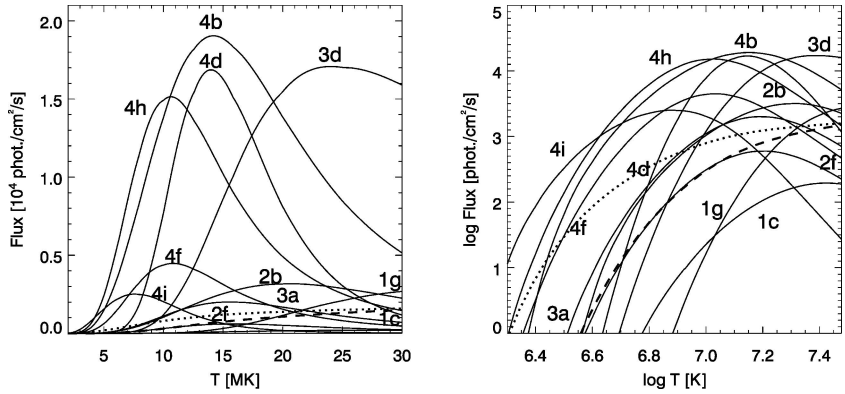

Figure 5. Calculated (Young *et al.*, 2003: CHIANTI) emission functions for the stronger lines observed by RESIK on linear (*left*) and logarithmic (*right*) scales. For potassium lines, interpolated values are given as derived from Kępa and Sylwester (2005). Coronal composition has been adopted and an emission measure $EM = 10^{48}$ cm^{-3} assumed. In case of the continuum flux calculations (*dashed line*, at 3.5 Å; *dotted line* at 6.0 Å), the width of the continuum narrow band $\Delta(\lambda)$ has been assumed to be twice the line width given as wavelength resolution in Table I.

RESIK has a number of subsidiary scientific objectives. For example, ionization fractions from solar X-ray line intensities may be empirically determined, so verifying ionization equilibrium calculations which involve a large amount of atomic data whose accuracy cannot be readily checked by other means. RESIK observations of line emission during long-duration flares or non-flaring active regions should be useful in this respect. It may also be possible to use RESIK to search for non-equilibrium conditions through line ratios.

4. The RESIK Instrument

The idea of an X-ray instrument for detailed spectroscopic studies of solar coronal plasma composition was conceived in the late 1980s in discussions involving the present RESIK consortium representatives. In spite of considerable political changes in the intervening time, the instrument was successfully designed, constructed, tested, and finally launched on the *CORONAS-F* spacecraft. This section describes the instrument in some detail. Notwithstanding the complete change of political circumstances that occurred during the instrument design, construction and testing periods, it was possible to finalize and launch the instrument described in more detail later.

4.1. Instrument concept, design, and operation

The RESIK instrument consists of two spectrometers (A and B) including front end electronics located in the open vacuum of space, and an electronics box including the instrument microprocessor located in a pressurized section of the spacecraft. Thermal filters (one for each spectrometer) prevent direct solar heat from entering the instrument. Diffraction occurs according to the Bragg law, $n\lambda = 2d \sin\theta$, where n is the diffraction order (1, 2, or 3), λ the wavelength of incident radiation, d the crystal lattice spacing, and θ the angle of incidence. Silicon and quartz, the crystal materials, with low atomic numbers, were chosen to reduce fluorescence of the crystals by solar X-rays (fluorescence yield is approximately proportional to Z^4) as much as possible. Fluorescence emission from the crystals forms a background to the spectra which for channels 1 and 2 is mostly insignificant. In channels 3 and 4 the fluorescence contribution can be accurately estimated (Section 4.7). This allows line-to-continuum intensity ratios (and therefore absolute element abundances) to be derived. In this respect, RESIK has an important advantage over the *Yohkoh* BCS which uses a germanium ($Z = 32$) crystal with a large fluorescence yield. The crystals were prepared, mounted, and characterized at the U.S. National Institute of Standards and Technology (NIST). X-rays diffracted from the crystals are detected by one-dimensional position-sensitive sealed proportional counters like those used for the *Yohkoh* BCS. A single detector is used for each spectrometer, i.e. there is one detector for two spectral channels. Each channel forms half of one detector, which

is electrically separated from the other channel by a cathode screen of grounded wires and has a pair of anode wires connected to a pre-amplifier. A high-voltage unit (HVU) supplies the necessary voltage (1.5 kV) to the anode wires. Position encoding is implemented using a lookup table (LUT), the position being given by the ratio of one of the cathode signals to the total signal. The data are binned into 256 bins for each detector and are passed to an accumulator which stores data in one buffer and simultaneously writes the data to telemetry. An ^{55}Fe source on a movable arm (the only movable part of the instrument) allows on-board calibration of the detectors. These calibrations, performed many times since spacecraft launch, allowed us to confirm that detector gain did not appreciably change over the period of operations.

The detectors, HV units, and electronics processing cards are spare units from the construction of the *Yohkoh* BCS. However, the RESIK spectrometer has significant improvements over the BCS in that the high-Z fluorescence background is eliminated and also there is capability to observe solar X-rays in diffraction orders higher than $n = 1$. This is achieved by appropriate adjustment of detector high voltages and discriminator settings (ADS) of the pulse-height analyzers. Periods of several days were chosen during 2002 and 2003 for RESIK observations in third-order ($n = 3$) diffraction. These periods are indicated by color codes on the RESIK Catalogue web pages *http://www.cbk.pan.wroc.pl/resik_catalogue.htm*. As a result, significant line emission was recorded during a number of flares at wavelengths $\lambda < 2$ Å (cf. Figure 14).

In designing RESIK, instrument sensitivity was traded with wavelength coverage. A compromise was chosen in which the wavelength coverage was large enough to include many emission lines of interest for abundance and differential emission measure studies yet with RESIK having a sensitivity that greatly exceeds those of the scanning flat crystal spectrometers on *SMM* or the *P78-1* spacecraft which covered the RESIK wavelength range. Instead of having a fixed data gathering interval (DGI) of, e.g., a few seconds, resulting in only a few hundred counts over the 1024 spectral bins, the on-board software was designed so that the DGI was dynamically determined by the on-board computer according to the level of solar X-ray emission in order to maintain count statistics. Thus, for the rise to a large flare, the DGI decreased from 5 min to only 1 s at flare maximum. An example of such observations with changing DGI is illustrated in Figure 6.

In order to increase the instrument sensitivity still further, RESIK has no collimator, so resembles the *Yohkoh* BCS (but not the Bent Crystal Spectrometer on *Solar Maximum Mission* which had a 6 arcmin FWHM collimator). This means that flares occurring anywhere on the Sun give rise to line emission in the detectors. There is consequently ambiguity along the dispersion direction whenever two or more flares occur simultaneously; however, this has been found to be an infrequent occurrence. The optical axis of RESIK is co-aligned with the spacecraft axis to high accuracy, achieved in pre-launch alignment tests. Thus the nominal wavelength ranges of the four detectors are slightly extended if a flare is considerably off-axis. Thus, the

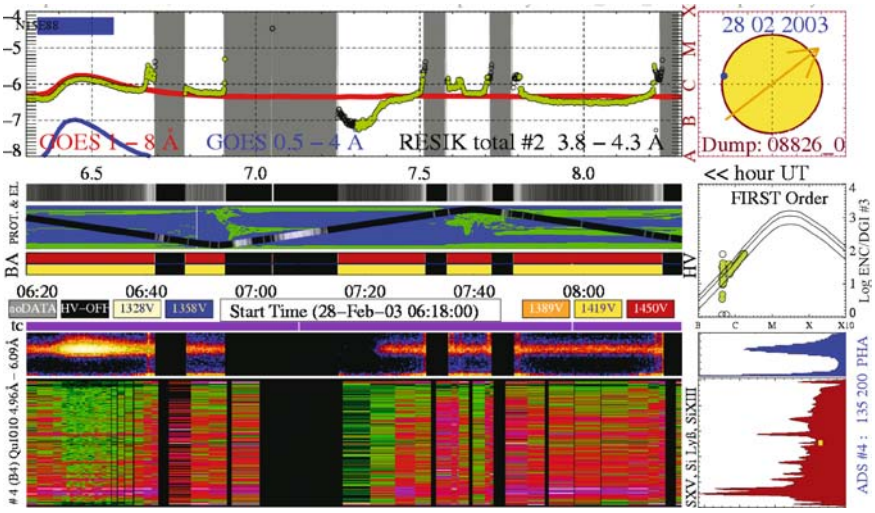

Figure 6. A portion of the RESIK Catalogue page available on line at the address *http://www.cbk.pan.wroc.pl/resik_catalogue.htm*. Many parameters are shown on the catalogue page including both the time-resolved spectra and PHA records, orbital position, spacecraft environment (day – night), particle contamination, crystal temperatures, etc. For details, see description at the *http://www.cbk.pan.wroc.pl/legend/legend_2003.htm*.

Ar XVII $1s^2\,{}^1S_0 - 1s3p\,{}^{1,3}P_1$ lines at 3.36 Å, normally shorter than the lower wavelength limit of channel 1, are occasionally visible within that detector's range. Also, because of the variety of flare dispositions on the Sun, the S XV $1s^2\,{}^1S_0 - 1s3p\,{}^1P_1$ line at 4.30 Å is sometimes visible at channel's 2 long-wavelength end, other times at channel's 3 short-wavelength end (see Table II).

Because of the high sensitivity of RESIK, large flares (*GOES* class X1 or greater) are liable to produce very high count rates and the detector's position encoding electronics saturate, producing distorted spectral information. The cathode electronics, having the longest time constant ($\sim$35 μs), are most affected. The RESIK detectors do not have line "narrowing" effects present for the *Yohkoh* BCS, whereby at high count rates emission line profiles are higher and narrower than usual (Trow, Bento, and Smith, 1994), but a small lowering of the PHA gain is observed for X-class flares.

4.2. Instrument Parameters

Table I lists relevant parameters of the RESIK instrument. The channel numbering follows that of previous publications, though for pre-launch testing and software purposes a different scheme is used (see Figures 3 and 4). Extreme wavelength ranges are for sources, observed off-axis by $\sim$20 arc min from disc centre. Values of dispersion, effective area, and wavelength resolution are given for mid-channel wavelengths.

TABLE I
Characteristics of RESIK channels.

	Channel 1	Channel 2	Channel 3	Channel 4
Detector	A	B	A	B
Software channel index	2	0	3	1
Crystal	Si	Si	Quartz	Quartz
Plane	111	111	$10\bar{1}0$	$10\bar{1}0$
$2d$ spacing (Å)	6.27	6.27	8.51	8.51
Bent radius (R, cm)	110.0	100.0	145.0	52.5
Length[a] (cm)	12.8	11.6	12.8	12.8
Detector edge to crystal edge distance[b] (X, cm)	3.74	4.66	4.12	4.75
Incidence angle range (°)	29.5 – 39.7	35.0 – 44.9	28.2 – 36.6	31.7 – 48.2
R_c – integrated reflectivity[c] (μrads)	53	52	21	18
Wavelength				
Nominal range[d] (Å)	3.40 – 3.80	3.83 – 4.27	4.35 – 4.86	5.00 – 6.05
Extreme range[e] (Å)	3.33 – 3.90	3.78 – 4.32	4.23 – 4.92	4.90 – 6.15
Wavelength resolution (mÅ)	8	9	12	17
Dispersion[c] (mÅ bin^{-1})	2.49	2.28	2.85	4.99
Principal lines in range	Ar XVIII, K XVIII	Ar XVII, S XV	S XVI	S XV, Si XIV, Si XIII

[a]Crystal lengths are actual crystal dimensions; only part of the crystal length illuminates the detector window for a source with given offset.
[b]Minimum distance between the detector and crystal, normal to the direction to source (X in Figure 4).
[c]Reflectivity and dispersion values are given for the first-order reflections and mid-channel wavelengths (see Figure 8).
[d]Nominal wavelength ranges are those recorded at all times, independent of the source offset.
[e]Extreme wavelength ranges are those seen for sources with largest offsets.

Instrument sensitivity or equivalently the effective area is an important quantity for the determination of emission measures, interpretation of ratios of line between channels, DEM determinations, and cross-calibration studies with other instruments such as the *Yohkoh* BCS and *RHESSI*. For a bent crystal spectrometer, the effective area is given by Rapley *et al*. (1977):

$$A_{\mathrm{eff}} = \frac{A_0}{\theta_1 - \theta_2} \frac{180}{\pi} \frac{\lambda}{2d} D R_c, \tag{1}$$

where A_0 is the crystal geometrical area, D the detector efficiency, R_c the crystal integrated reflectivity (radians), and θ_1 and θ_2 the Bragg angles at each end of each

crystal. The detector efficiency was calculated using the following construction details:

- Kapton thermal filter thickness $12.5 \pm 1.0\,\mu$m with 900–1200 Å aluminum coating,
- detector Be filter thickness $125 \pm 4\,\mu$m,
- detector gas absorption length 20 mm, gas pressure 1.2 Atm ± 10% .

The detector efficiency calculations and corresponding error analysis indicate that the absolute uncertainties are only few percent over the energy range of interest, between 1Å and 7 Å.

4.3. CRYSTALS

The problem of obtaining accurate values for crystal reflectivities is the most difficult in the instrument calibration. End-to-end RESIK tests carried out at Rutherford Appleton Laboratory and Mullard Space Science Laboratory over a 3-month period in 2000 allowed measurements of the crystal reflectivities. In these tests, a vacuum chamber previously used for the calibration of the *Yohkoh* BCS was used, but with an improved double crystal X-ray monochromator. However, these calibration data still await analysis. Meanwhile, crystal reflectivity data available from other sources were investigated. We made use of theoretical codes from the World Wide Web, though laboratory measurements of R_c for silicon or quartz crystals do not seem to be available. Among the theoretical codes are the early reflectivity calculation of Brennan and Cowan (1992) for selected wavelengths and reflection orders. We also accessed two independent crystal codes written by Lugovskaya and Stepanov (1991) and Dejus and del Rio (the XOP code, 1996). All three codes provide R_c for flat crystals as a function of wavelength over the RESIK range of interest. However, only the XOP code permits calculation of crystal reflectivities in the case of bent crystals, as used in RESIK.

In Figure 7, we compare the three sets of calculations for integrated crystal reflectivities. It can be seen from the figure that the results from the three independent crystal codes agree well. The differences are within few percent for the first-order reflection. The same applies to results for third-order reflection. We found that the results agree well in the case of flat crystals. Bending quartz crystals increases the total reflectivity substantially for second-order reflections below 3 Å (by up to 50%) and changes dramatically the R_c for both silicon and quartz in third order (by a factor of ∼5). This causes the second-order quartz reflectivity to be similar to the first-order reflectivity, something that was not expected in the RESIK design phase. This is likely to lead to contamination of RESIK third-order spectra. Investigations into this are in progress. It can be seen from Figure 7 that the crystal reflectivities are large enough in second and third orders to measure substantial line emission at short wavelengths ($\lambda = 1.2$–3.1 Å) in large flares, enabling high-temperature lines to be observed, notably the group at 1.85 Å consisting of Fe XXV plus satellite

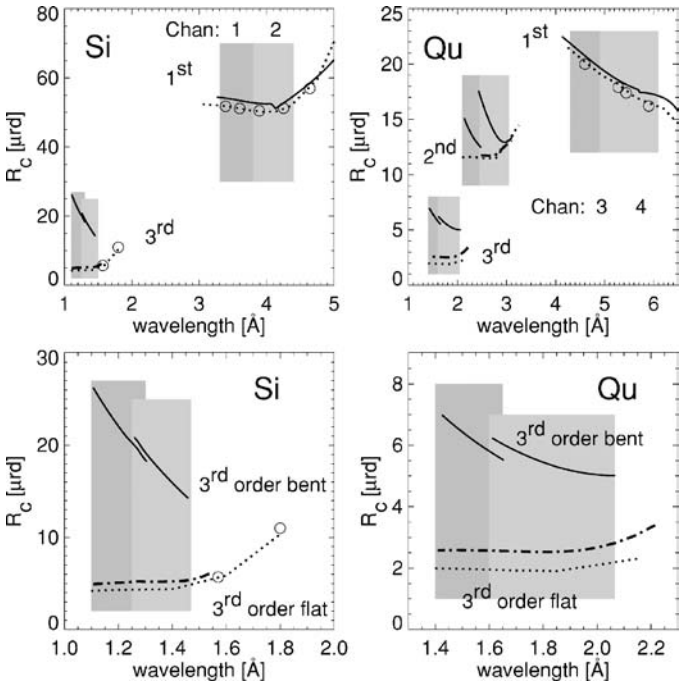

Figure 7. Calculated integrated reflectivities of RESIK crystals in first, second, and third reflection orders. Note that second-order (222) reflections are forbidden for silicon crystals. Results from Brennan and Cowan (1992) code (*open circles*) are overplotted on the *dotted line* showing results obtained from Stepanov code (Lugovskaya and Stepanov, 1991). *Continuous line* represents the XOP calculations (Dejus and del Rio, 1996) made for the crystal bent according to RESIK specifications, while *dot-dashed lines* represent the XOP results at the "flat crystal" limit. See the text for discussion.

lines. By combining calculated detector efficiencies and crystal reflectivities, the instrument effective areas have been calculated according to Equation (1), using the construction data from Table I. The results are presented in Figure 8.

4.4. Detectors

The instrument uses two double position-sensitive proportional counters that detect soft X-rays reflected from the four spectrometer crystals. The detectors are identical to those used in the *Yohkoh* BCS instrument (Lapington *et al*., 1990; Culhane *et al*., 1991; Trow, Bento, and Smith, 1994) designed and made at the Mullard Space Science Laboratory.

The main feature of the detector is its one-dimensional position-sensitive readout. The detector is optimized for detection of X-rays in the 2–7 keV energy range, and for use in a space environment. It features low mass, small volume, low power consumption, and long life. Preamplifiers and test circuitry are mounted in

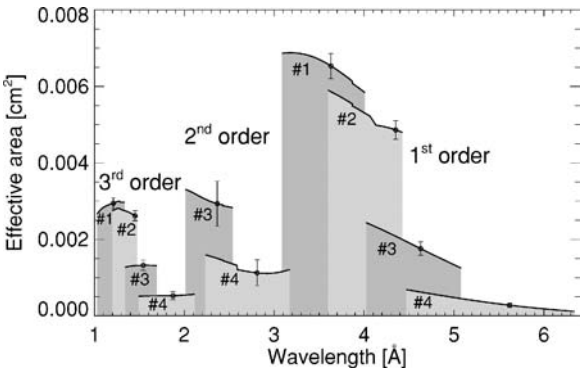

Figure 8. The calculated effective area of all RESIK channels, in all available orders of reflection, shown as a function of wavelength. The default observing mode (first order) covers the range 3.25–6.15 Å. Same shades represents common detectors: lighter – detector A, darker – detector B.

a package on the rear of the detector. No gas supply system is required, as the detector is sealed permanently. The gas filling is an equal xenon–argon mixture with 5% CO_2 as a quench agent. The pressure of the gas filling is 1.2 atm at 20 °C. This mixture of gases was chosen to provide the required quantum efficiency, signal characteristics and aging properties. The detectors are powered from external high-voltage supplies made at Rutherford Appleton Laboratory, to establish the anode wire fields.

When a photon enters one of the detectors, it emits shaped analogue pulses which are further processed to yield the event positions. The detector has two anode channels so it is used to observe spectra diffracted from the two crystals simultaneously. The detector is essentially a hollow stainless steel rectangular box (see Figure 4), with a thin beryllium foil (125 μm), semi-transparent to X-rays forming one of the larger faces. Thin metal wires are suspended along the centre of the box, and high voltage is applied to these wires (the anodes). Other electrodes (cathodes) are placed in the detector immediately behind the anodes. They enable the position to be read out and are held at ground potential. Each ionization within the detector volume produces charges deposited on the anode. A charge-sensitive preamplifier is connected to the anode and the number and approximate energy of incident photons can be determined from the measured signal amplitude. The position-sensing capability of the detector is accomplished by the backgammon technique (so called because configuration of the readout cathodes' interleaved wedges, resembles a backgammon game board). When an avalanche occurs at the anode, charges are also induced on the wedges. The amount of charge on each of the two electrodes depends on the position of the event and these induced signals are used to determine the position, in one dimension, of the event.

The detector is mounted in the spectrometer by means of attachment points on the upper (window) side (see Figure 4). In its flight configuration, an electronics

package is integrated with the detector, and this package has an alloy enclosure and cable harnesses. The window frame has a recess into which the window is bonded, and an attachment point for the gas filling tube. The detector is fixed to the spectrometer by means of four feet, which are part of the window assembly. A vibration-damping mounting system is used, consisting of small O-rings and continuity straps. This isolates the detector from vibrations and the structure (at launch and at other times during assembly and integration) whilst preserving alignment and maintaining electrical continuity.

X-rays enter the detector through its window, which is a single piece of 125 μm beryllium foil brazed to the window frame. Although the window is securely attached to the window frame, the strength of the beryllium foil is insufficient to support the outward pressure, and therefore the window frame has a number of apertures cut into it, leaving bars arranged along the length of the detector. These bars have sufficient rigidity and are closely enough spaced to support the window. These bars reduce the active area of the detector by 20%. Because they are parallel to the position-sensing axis of the system, the presence of these bars has no other effect in the spectra. The anodes are connected together in pairs, by conductors (inside the detector, but outside of the internal end walls). The anodes are 15 μm diameter alloy wires (92% Pt and 8% W). The detector volume is divided into two cells by a set of cathode wires. These wires are equally spaced along a line which divides the cross-section of the detector into two equal parts. The effect of these cathodes on the electric field is the same as if a solid conductor were to divide the detector. The potential is zero at the cathodes, and so the field configuration is symmetrical. The counter thus functions as two separate detectors.

The position-sensing function of the detector is provided by the wedge-and-wedge cathode plate. This is a fused silica (quartz) plate, 2 mm thick, with a thin gold layer deposited onto it. A continuous line is etched into the conducting layer, dividing it into two electrodes (the wedges). When the detector is operated, a charge distribution is induced onto this cathode whenever there is an avalanche on the nearby anode wires. The wedges act to divide the quantity of induced charge according to the position of the avalanche. The signals from the wedges are digitized to 8-bits, and are routed through the LUT to determine the position of each event to within a fraction of 1 mm (the spectrometer electronics unit carried out this function using the LUT stored in the EPROM memory).

This method of signal processing is advantageous in space-engineering terms, but has some drawbacks. These are mainly related to the degree of uniformity seen in the encoded data. At certain positions, it appears as if there are spikes and notches in what should otherwise be a flat or smoothly varying pattern of illumination (cf. Figure 12). This is most pronounced at the centre of the readout, and is clearly visible at approximately one quarter and three quarters of the distance along it, and also results in less pronounced non-uniformities elsewhere. These are seen in the RESIK data and were also a feature of *Yohkoh* BCS spectra (see The *Yohkoh* Analysis Guide, 1999) and the BCS on *Solar Maximum Mission*. These non-uniformities are due

to the way in which analogue-to-digital converter (ADC) output data is processed by the instrument position-encoding LUT. This is because the LUT implements a analogue-to-digital division operation at a fixed arithmetic precision. The *Yohkoh* BCS and RESIK LUT store the result of the following expression in the LUT address:

$$(W_1, W_2) : 256W_1/(W_1 + W_2). \tag{2}$$

If the result is not exact, then the nearest integer value is used. The nature of the resulting redistribution function, from real position to encoded position is not smoothly varying, and the result is that spikes and notches are added to the spectrum. The effect was referred to as the "notch" effect in discussions of BCS spectra from *Yohkoh* and *SMM*, though it is more properly called a *Fixed Pattern Structure* (FPS) since the effect can influence any bin in the data and not only certain positions along the LUT map. It should be noted that the structure of FPS depends on the locations being sampled by the ADC data, i.e., on the given ADS and HV values, and is somewhat data dependent. Technically, it is not a true fixed pattern, and cannot truly be removed by scaling by a constant flat field. However, for practical comparison of spectra, a convenient approximation has been developed in order to correct for such a scaling. This is possible since the appearance of the structure is relatively stable over a range of observations obtained with similar ADS and HV settings. Computation of the FPS pattern has been followed successfully allowing to correct for this effect. This work was done by Phillips (1994) and recently by Sylwester *et al*. (2004a), for the *Yohkoh* BCS and RESIK instrumentation setups, respectively. It should be noted that the mechanism of the effect is not a scaling law (like a sensitivity change) but a redistribution of counts from one location, inaccessible due to the finite table, to another. In general, no counts are lost due to the encoding process. For purposes of spectra reduction, we incorporate experimentally determined FPS corrections, different for each ADS and HV settings, i.e., the for each spectral observing mode.

The position-sensing function of the encoding system becomes electronically saturated when the count rates exceed few thousand counts per second. The saturation enable the spectra to be seen only for flares below the M8 and X1 *GOES* importance class for detectors A and B, respectively.

Each detector may be illuminated, when required, by an Fe^{55} calibration source. The stepper motor assembly which moves the calibration source can be seen in the upper part of the instrument box shown in Figure 4. On command, the calibration source is rotated so as to flood the detector window uniformly with the characteristic X-rays of the decay of this isotope (Mn Kα_1 and Kα_2 at 5.899 and 5.888 keV, respectively). Data from such calibration activities has not indicated any appreciable change in the detector gain (a measure of the detector gas integrity) over the duration of the experiment.

4.5. Comparisons of RESIK data with other instruments

A great deal of attention has been paid to the intensity calibration of the RESIK spectrometer, and we believe the effective areas shown in Figure 8 are accurate to about 20% or better in the first diffraction order. It is possible to verify this by comparison with X-ray data from other solar X-ray instruments. Unfortunately, there is less than 5 months of overlap between the launch of *CORONAS-F* (31 July 2001) and the loss of communication with the *Yohkoh* spacecraft (14 December 2001). However, during this time several flares occurred which will enable comparison of data from the *Yohkoh* Bragg Crystal Spectrometer, which includes spectra from the range of the Fe XXV ($\lambda \sim 1.9$ Å), Ca XIX lines ($\lambda \sim 3.17$ Å), and S XV lines ($\lambda \sim 5.04$ Å). Analysis of simultaneous data sets is proceeding at present.

It has been possible to compare data from the *Reuven Ramaty High Energy Solar Spectroscopic Imager* (*RHESSI*) with RESIK data. *RHESSI*, which was launched on 5 February 2002, observes the X-ray and gamma-ray spectra of solar flares from 3 keV to 17 MeV, with an energy resolution of 1 keV or slightly better in the X-ray region. Two atomic line features, viz. the group of Fe XXV lines and satellites at 1.9 Å (6.7 keV) and higher-excitation Fe XXV lines and Ni XXVII lines at 1.58 Å (7.9 keV), are observed as broad features on a continuum. The thermal continuum can be traced in flare spectra to very high energies ($\sim$30 keV) where, at the flare impulsive stage, a non-thermal bremsstrahlung continuum appears Lin *et al*. (2002). The continuum observed by *RHESSI* at its low-energy end, $\sim$3 keV (4 Å) can be compared with that observed by RESIK in channels 1 and 2 where the fluorescence contribution to the background is considered to be very small.

The double-peaked flare on 26 April 2003, with maxima in the *GOES* X-ray emission at 03:05 UT and 03:08 UT, is an example when RESIK and *RHESSI* spectra can be compared. During this flare, the RESIK instrument was set to a third-order spectrum mode in the interval 03:03:40 UT to 03:11:40 UT. RESIK first-order spectra are available over the period from 02:27 UT till the end of the flare, at about 03:20 UT. Figure 9 shows on a photon energy scale RESIK first-order spectra (channels 1–4) at 03:00 UT and simultaneous *RHESSI* spectrum. The effective areas shown in Figure 8 were used to convert photon count rates to absolute fluxes. The *RHESSI* spectrum, derived from standard *RHESSI* analysis software, becomes increasingly uncertain at the lower-energy (3–4 keV) part of its spectral range, but even so there is $\leq$15% difference between the continuum as observed by channels 1 and 2 of RESIK (photon energy range 2.9–3.7 keV) and that observed by *RHESSI*. There is a fluorescence contribution to RESIK channels 3 and 4 (2.0–2.9 keV) which appears to enhance the continuum in this range. Allowing for this, the *RHESSI* continuum slope very closely matches that of the RESIK continuum slope.

In the short interval when RESIK observed in third order, the group of Fe lines at 1.9 Å were observed. Over the period 03:03:12–03:05:32 UT, the averaged Fe-line flux, obtained using third-order diffraction effective areas from Figure 8,

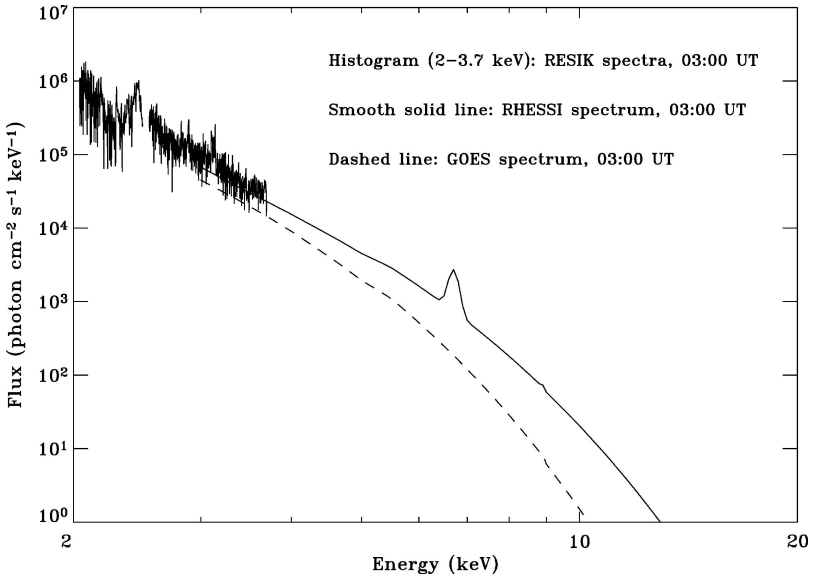

Figure 9. Comparison of RESIK, *RHESSI* and *GOES* spectra during the M2.1 flare on 26 April 2003. The spectra are plotted against energy (keV) and the spectral fluxes are in units of [photons cm^{-2} s^{-1} keV^{-1}]. The RESIK spectra include all four channels and cover the range 2.04–3.68 keV (i.e. 3.37–6.09 Å). The *RHESSI* spectrum is from spectral fits to the data using the standard *RHESSI* spectral software package. The *GOES* spectrum is calculated based on the temperature and emission measure derived from the ratio of the two *GOES* channels inserted into a function describing only the thermal continuum (free–free and free–bound) emission.

is ∼82 000 photons cm^{-2} s^{-1}. This compares with ∼61 000 over the same period from the *RHESSI* software, in which the flare's spectrum is analyzed using a thermal continuum function and two Gaussian line features to fit the 6.7 keV (Fe line) and 7.9 keV (Fe/Ni line feature). The agreement is satisfactory.

These and other comparisons of the spectra, being made at present, give confidence to our intensity calibration determination which appear to be accurate to 20% as stated.

4.6. Orbital background

RESIK detectors have been operating without interruption for nearly 2 years, with the high voltage (HV) turned off (since late 2001) during passages of regions with high energetic particle densities. These include the polar auroral ovals (AO), because of the spacecraft's high-inclination orbit, and the South Atlantic Anomaly (SAA). In particular, the signal has been measured from each of the four detector channels during spacecraft (S/C) nights. During this night portions of the orbit, the observed signal is made up of the following sources:

– slowly varying, low-intensity orbital particle background which level depends on S/C geomagnetic coordinates,
– intense particle background, nearly saturating the detectors observed during passages of the SAA and polar ovals,
– low-to-medium intense X-ray background, most probably due to direct anisotropic illumination of the detector window by the ionospheric X-ray emission generated *in situ* within the AO plasma,
– emission from a direct illumination of the detector by non-solar strong X-ray sources like Sco X-1.

The slowly varying orbital particle background is observed to have a well-defined spectrum, nearly independent of the S/C coordinates. Its shape depends somewhat on the detectors' HV and ADS settings. In Figure 10, an example of this orbital background is shown, as seen in all spectral channels bin rates during first 2 weeks of January 2003. The spectra have been collected over a period of ∼18 h including ∼80 clean night portions of the satellite orbit. The plot clearly shows peaks within 10-bin end portions of spectral ranges corresponding to so-called hidden bin areas (cf. Figure 4, right panel). In these hidden bin areas no illumination by X-rays diffracted from the crystal is possible. The signal in these hidden bin areas can only come from the above "contaminating factors". The configuration of the position-encoding system is such that the bins in these areas correspond to a greater physical length of the detector than the other bins. Each hidden bin corresponds to a length approximately five times that of a bin in the central area. This causes the appearance of intensity enhancements at both ends of the detector, seen as peaks in Figure 10. The signal from the hidden bins is mostly due to background particles, and because of the detector position sensitivity, this particle rate is very low, less than 0.01 cts (bin s)$^{-1}$. This low background means that RESIK sees true continuum levels for solar sources with emission measure as low as 10^{46} cm^{-3} (at $T = 10$ MK). It is possible, given the height of the hidden bins, to estimate

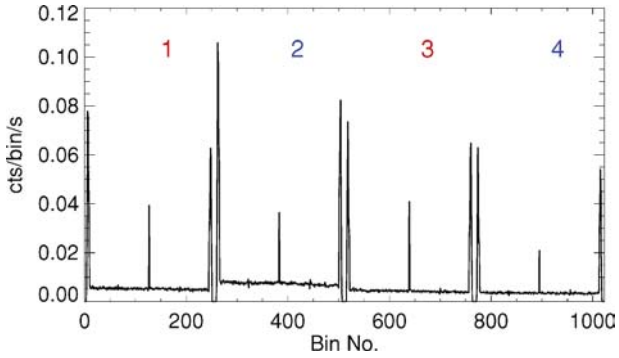

Figure 10. Observed rate of the low-intensity orbital background collected over ∼1.5 × 10^5 s early in 2003. The numbers denote respective RESIK channels.

(and subtract) the contribution to the measured spectra of the particle background component. This correction is incorporated within the spectra reduction software written in Interactive Data Language (IDL) and known as *RESIN*. Also during the S/C day, by monitoring the height of the hidden bin signal, it is possible to remove the background contamination. Investigation of relative heights of the signal measured in a pair of hidden bins in each channel allows us to identify the presence of the other sources of background contributors. Both auroral oval and non-solar X-ray direct illumination of the detectors causes an increase in the signal in one of the hidden bin areas (near bin 5). This asymmetry of the intensity in the hidden bin regions is tracked, and this can be used to select, during analysis, only those spectra where no unwanted contamination is present. In order to increase the lifetime of the detectors, the high voltage was switched off during passages of the spacecraft orbit through the SAA and AO regions of Earth's magnetosphere. To enable triggering of the HV switch off, the read-outs from the four PIN radiation particle environment sensors were used (see Figure 3 for location of these sensors).

The sensitivity of these PIN detectors was found to correlate best ($r \sim 0.97$) with the high energy ($E > 26$ MeV) proton flux as measured concurrently by MKL, a part of the SKL instrument also aboard *CORONAS-F*. The correlation diagram showing this direct relationship is presented in Figure 11. The right panel in the figure illustrates the distribution of the high-energy background protons seen by the RESIK PIN detectors in May 2002. Clearly, the most contaminated are regions within the polar ovals, in addition to the well-known SAA. During the first 3 months of the mission's lifetime, the RESIK instrument was closely monitored with the amplitude discriminators set to the widest possible range, but as experience was gained we were able to design a special software routine, uploaded to the instrument's on-board computer which allowed the HV unit to be switched off during high particle density periods. The data from the PIN detectors are being analyzed in order to find out by how much the energetic particle environment in the SAA and AO regions depends on the solar activity (Kowalinski *et al.*, 2004).

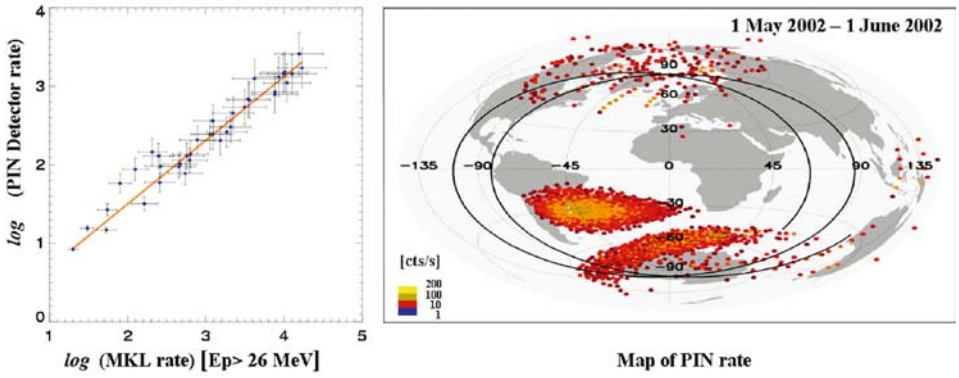

Figure 11. *Left*: correlation diagram between PIN and MKL rates. *Right*: distribution of rates as seen by RESIK PIN detectors in May 2002.

4.7. FLUORESCENCE CONTAMINATION

We found that, in spite of taking the precaution of using silicon and quartz crystals (i.e., material with low atomic number, $Z = 14$, and thus small fluorescence yield), there was a substantial fluorescence in RESIK spectra. With the *SMM* and *Yohkoh* bent crystal spectrometers, a germanium crystal was used ($Z = 32$), giving a high fluorescence background (fluorescence yield is approximately proportional to Z^4). Our pre-launch expectations were that use of silicon and quartz crystals would reduce this background by a factor of 30. The low-energy threshold for Si K-shell fluorescence is $E = 1.84$ keV; the transmission of the beryllium detector window is 5% or less at this low energy. However, the X-ray spectra of flares and active regions still have large numbers of photons above 1.84 keV, causing the RESIK crystals to fluoresce and giving rise to a background emission of Si Kα photons with energy 1.75 keV. These photons form a background emission to the RESIK solar spectra. This background is always present, but its level varies depending on the ADS and HV settings at the time.

When the importance of fluorescence was first realized, a special sequence was devised in which the ADS and HV settings were adjusted so that the fluorescence signal in the pulse height analyzer was just separated from the solar signal. Over the period 30 August –5 September 2002, the RESIK instrument was run in this fluorescence calibration mode, collecting more than 300 time intervals, total duration 34 h, when the fluorescence and solar spectra were measured. During this time, solar activity on the *GOES* scale varied from B2 to over X1. The resulting summed fluorescence spectrum is shown in Figure 12. It was found that the shape of the fluorescence spectrum does not depend significantly on the level of solar activity. This has helped us to develop an algorithm to correct for the fluorescence.

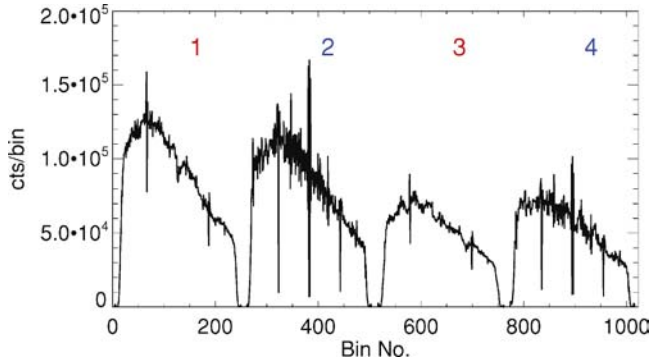

Figure 12. Observed profile of the fluorescence from the RESIK crystals. The spectrum shown was integrated over a 34 h period between August and September 2002. The numbers at the top of the figure denote channel number. Note that the observed fluorescence signal is two times higher for channels (1 and 2) with silicon crystals than for channels (3 and 4) with quartz crystals.

Depending on the ADS and HV settings, only part of this fluorescence spectrum contaminates the measured spectrum. With known detectors' characteristics (i.e., the energy resolution and energy dependence of the fluorescence peak position in the ADS scale), the contaminating fraction can be precisely calculated. During each spectra gathering interval, independent information is also available on the integrated flux observed in the fluorescence peak at 1.75 keV. This information comes from the PHA 32-bit amplitude analyzer, where Si fluorescence contributes to the dominating low-energy component peak. With the total fluorescence rate and the calculated fluorescence fraction leaking to the observed spectra known, the detailed fluorescence contamination profile can be calculated, and subsequently subtracted from the measured spectrum. The operation of the algorithm correcting for fluorescence was verified even when the real solar spectrum is only few percent of the total

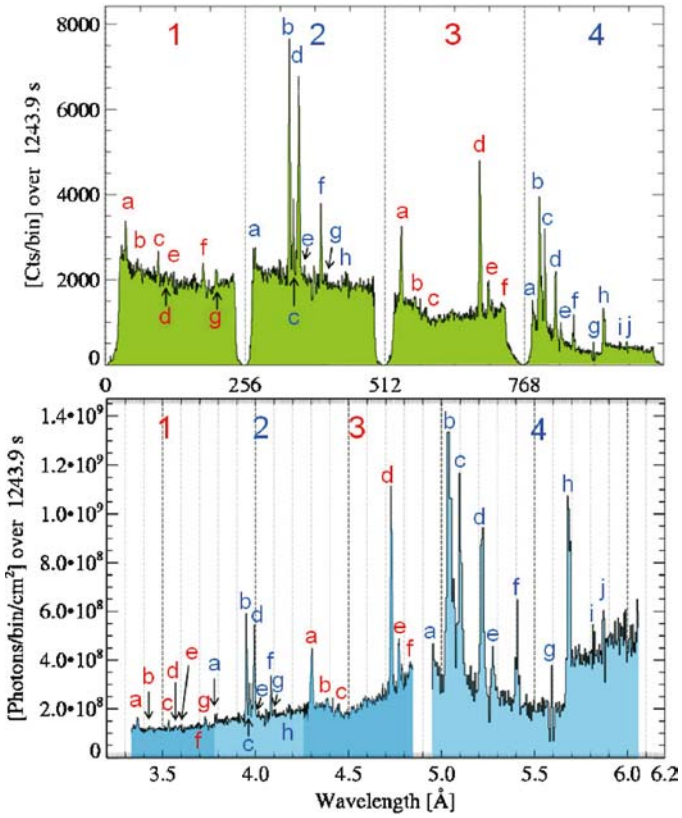

Figure 13. Example composite RESIK spectra as measured (*upper panel*) and after reduction (*lower panel*). During the reduction process, orbital background and fluorescence contamination have been removed. The spectra cover the wavelength range 3.35 – 6.15 Å and were collected during the 20 min rise phase of the M1.9 east-limb flare on 21 January 2003. For each channel, the key letters above spectral features refer to those listed in Table II where spectral identifications are given.

spectral signal. The fluorescence removal process will be described in more detail elsewhere (Sylwester *et al*., 2004b). The fluorescence removal algorithm is already built into the *RESIN* spectral reduction package (Kowalinski and Sylwester, 2004).

The fluorescence contamination is the most serious for RESIK channels 3 and 4. For channels 1 and 2, the contribution is never more than few percent (with the exception of the period August–September 2002 when the fluorescence was being investigated). During the early part of the instrument operations, the instrument ADS and HV settings were adjusted several times so that the fluorescence in channels 3 and 4 was minimized. By late 2002, optimum settings were achieved, and it was found (for these settings) that the fluorescence contribution was not higher than ∼20%. Most of the analysis of RESIK data done so far is after this time.

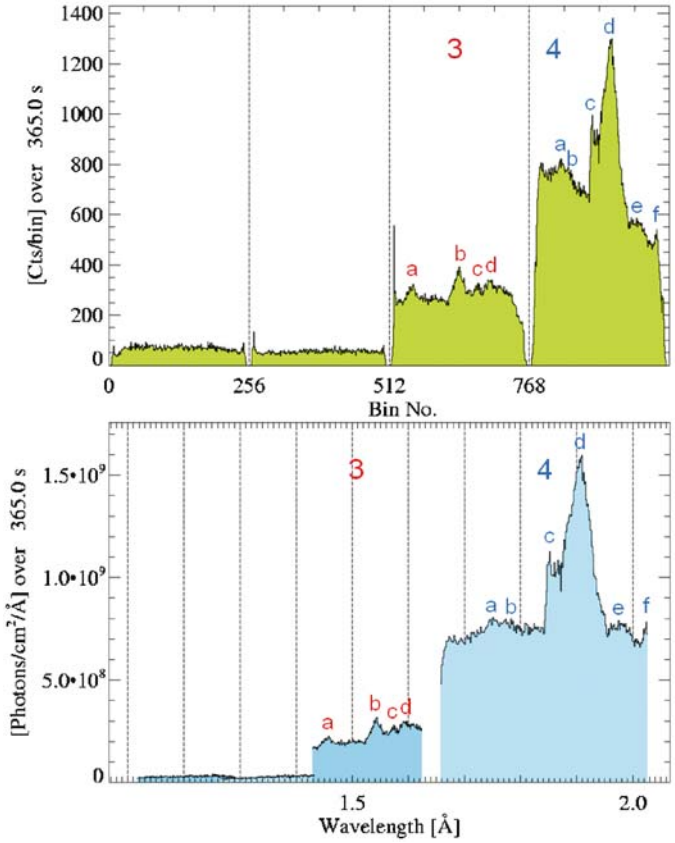

Figure 14. Example RESIK spectra measured in the mode where detectors were sensitive to photons diffracted from the crystals in second and third order. As a result, the reduction is more complicated. The spectra shown cover the wavelength range 1.35–2.05 Å and were collected during the maximum phase of the M2.1 flare on 26 April 2003. The key letters above spectral features refer to those listed in Table III where possible spectral identifications are given.

TABLE II
First-order spectral features.

Key	λ (Å)	T_m (MK)	Ion	Dominant transition
Channel 1				
1a	3.36	22	Ar XVII	$1s^2\,{}^1S_0 - 1s3p\,{}^{1,3}P_1$
1b	3.43	19	Ar XVI	*Satellite* to [1a]
1c	3.53	26	K XVIII	$1s^2\,{}^1S_0 - 1s2p\,{}^1P_1$
1d	3.57	19	K XVIII	$1s^2\,{}^1S_0 - 1s2s\,{}^3S_1$
1e	3.59	17	K XVII	*Satellite* to [1c]
1f	3.70	26	S XVI	$1s\,{}^2S_{\frac{1}{2}} - 5p\,{}^2P_{\frac{3}{2},\frac{1}{2}}$
1g	3.74	36	Ar XVIII	$1s\,{}^2S_{\frac{1}{2}} - 2p\,{}^2P_{\frac{3}{2},\frac{1}{2}}$
Channel 2				
2a	3.79	26	S XVI	$1s\,{}^2S_{\frac{1}{2}} - 4p\,{}^2P_{\frac{3}{2},\frac{1}{2}}$
2b	3.95	22	Ar XVII	$1s^2\,{}^1S_0 - 1s2p\,{}^1P_1$
2c	3.97	22	Ar XVII	$1s^2\,{}^1S_0 - 1s2p\,{}^3P_{1,2}$
2d	3.99	22	Ar XVII	$1s^2\,{}^1S_0 - 1s2s\,{}^3S_1$
2e	4.02		?	
2f	4.09	16	S XV	$1s^2\,{}^1S_0 - 1s4p\,{}^1P_1$
2g	4.10	14	S XIV	*Satellite* to [$1s^2\,{}^1S_0 - 1s5p\,{}^1P_1$]
2h	4.18	35	Cl XVII	$1s\,{}^2S_{\frac{1}{2}} - 2p\,{}^2P_{\frac{3}{2},\frac{1}{2}}$
Channel 3				
3a	4.30	15	S XV	$1s^2\,{}^1S_0 - 1s3p\,{}^1P_1$
3b	4.39	14	S XIV	*Satellite* to [3a]
3c	4.44	19	Cl XVI	$1s^2\,{}^1S_0 - 1s2p\,{}^1P_1$
3d	4.73	24	S XVI	$1s\,{}^2S_{\frac{1}{2}} - 2p\,{}^2P_{\frac{3}{2},\frac{1}{2}}$
3e	4.77		?	
3f	4.83	14	Si XIV	$1s\,{}^2S_{\frac{1}{2}} - 5p\,{}^2P_{\frac{3}{2},\frac{1}{2}}$
Channel 4				
4a	4.96	24	Si XIV	$1s\,{}^2S_{\frac{1}{2}} - 4p\,{}^2P_{\frac{3}{2},\frac{1}{2}}$
4b	5.04	13	S XV	$1s^2\,{}^1S_0 - 1s2p\,{}^1P_1$
4c	5.10	14	S XV	$1s^2\,{}^1S_0 - 1s2s\,{}^3S_1$
4d	5.22	14	Si XIV	$1s\,{}^2S_{\frac{1}{2}} - 3p\,{}^2P_{\frac{3}{2},\frac{1}{2}}$
4e	5.28	15	Si XIII	$1s^2\,{}^1S_0 - 1s5p\,{}^1P_1$
4f	5.40	11	Si XIII	$1s^2\,{}^1S_0 - 1s4p\,{}^1P_1$
4g	5.59		?	
4h	5.68	10	Si XIII	$1s^2\,{}^1S_0 - 1s3p\,{}^1P_1$
4i	5.82	7	Si XII	*Satellite* to [4h]
4j	5.87		?	

TABLE III
Third-order spectral features.

Key	λ (Å)	T_m (MK)	Ion	Dominant transition
Channel 3				
3a	1.457		?	
3b	1.542	180	Ni XXVIII	$1s\,^2\mathrm{S}_{\frac{1}{2}} - 2p\,^2\mathrm{P}_{\frac{3}{2},\frac{1}{2}}$
3c	1.571	60	Fe XXV	$1s^2\,^1\mathrm{S}_0 - 1s3p\,^1\mathrm{P}_1$
3d	1.591	80	Ni XXVII	$1s^2\,^1\mathrm{S}_0 - 1s2p\,^1\mathrm{P}_1$
Channel 4				
4a	1.750	–	Fe Kβ	
4b	1.781	150	Fe XXVI	$1s\,^2\mathrm{S}_{\frac{1}{2}} - 2p\,^2\mathrm{P}_{\frac{3}{2},\frac{1}{2}}$
4c	1.850	54	Fe XXV	$1s^2\,^1\mathrm{S}_0 - 1s2p\,^1\mathrm{P}_1$
4d	1.910	30	Fe	Many blended
4e	1.980	?		
4f	2.025	?		

5. Observations of the Flare of 21 January 2003

We illustrate the many thousands of RESIK spectra obtained since launch with an average one built up from ∼100 individual spectra during the 20 min rise of a typical flare, on 21 January 2003. This flare, with *GOES* intensity M1.9, occurred on the Sun's east limb (S07 E90). Spectra from all four channels are given in Figure 13. For the spectrum shown in the figure, orbital background has been subtracted and the fluorescence and FPS effects have been corrected for. The flare's position on the Sun gave rise to a large offset resulting in relatively small wavelengths (such as the Ar XVII 3.367 Å line) being observed. Note that on this occasion the S XV 4.299 Å line appears at the short-wavelength end of detector 3. Features identified with labels in the figure are deemed real solar lines, not instrumental artifacts such as FPS corrections or irregularities in the background. Table II contains some 34 lines with their tentative identifications. For strong lines, the identifications are obvious. With theoretical wavelengths of these lines, wavelengths of other, less strong lines have been found from geometry optimization, described earlier. This is justified as a very good first approximation since the crystal surface appears close to cylindrical over the greater part of each channel. For occasions when RESIK was in third order, the lines listed in Table III were detected. Figure 14 shows third-order spectra for the flare of 26 April 2003. There is a possibility of contributions from second-order diffraction for channels 3 and 4 (with the quartz crystal); this is under investigation at present.

6. Summary, Conclusions and Future Work

We have described the unique RESIK Bragg bent crystal spectrometer, part of the science package of the Russian *CORONAS-F* spacecraft. RESIK has collected over 500 000 spectra of flares, active regions and "quiet corona" over approximately 2 years of its operation since launch on 31 July 2001. At present its operation is suspended by problems with the power supply. Some of the details concerning the operation of the instrument may be found in the RESIK Weekly Newsletters (2002/2003).

RESIK has one of the better-understood calibrations of instrumental response among Bragg crystal X-ray spectrometers in solar physics. With its wavelength coverage it is very well suited to provide input for "experimental" cross-calibration of the previous (BCS *Yohkoh*) and recent (*RHESSI*, SPIRIT) X-ray solar mission. Over the entire duration of the RESIK active period, *GOES* soft X-ray measurements of the global solar flux are available in two bands: 0.5 – 4 Å and 1 – 8 Å from *GOES-8* (until April 2004) *GOES-10* and *GOES-12* (from March 2003). This offers the possibility of cross calibration between RESIK and the three *GOES* satellites. Such a comparison may lead to "observational" verification and/or improvement of the *GOES* temperature scale assigned to particular measured flux ratios for all early observations, starting around 1970.

Scientific issues being presently addressed in the ongoing analysis of RESIK data include:

- Identification of tens of new lines observed in the spectral range between 3.3 and 6.1 Å.
- Determination of coronal plasma composition and its variations in time and between events.
- Determination of differential emission measure distribution for flares and active regions.
- Determination of the "experimental" emission functions for important X-ray lines.
- Verification of available ionisation equilibria calculations.

All the RESIK data have been placed in the public domain and are available on request. The catalogue of RESIK observations is available online at the web address: *http://www.cbk.pan.wroc.pl/resik_catalogue.htm*.

Acknowledgements

The construction of RESIK has been possible thanks to enthusiasm of many people including M. Oczyński and E. Stańczyk (deceased) from Poland. We acknowledge financial support for RESIK from the Polish funding agency KBN (grants 2.P03D.024.17, 2.P03D.002.22 and PBZ-KBN-054/P03/2001) and the Exchange Visitors Programme of The Royal Society – Polish Academy of Sciences for travel

expenses. Gaps in the funding in the final 2 years of the project before the spacecraft launch were generously filled by several organizations and individuals listed in the Space Research Center's web site (*http://www.cbk.pan.wroc.pl/sponsor.htm*).

KJHP thanks the award of a US National Research Council Research Associateship at NASA Goddard Space Flight Center. Thanks are due to Dr. Brian R. Dennis for help with *RHESSI* spectral analysis. We acknowledge access to the *CORONAS-F* spacecraft attitude data (shown in Figure 2) which were obtained from Dr. Sergey Kuzin of the SPIRIT Team, FIAN, Moscow. In calibrating RESIK PIN sensors, we used SKL fluencies kindly provided by Dr. Alexander Podorolsky from MGU, Moscow. Anna Kępa is acknowledged for plots of line-emission functions.

References

Antonucci, E.: 1989, *Solar Phys.* **121**, 31.

Bentley, R. D.: 1999, *Yohkoh Analysis Guide*, *http://surfwww.mssl.ucl.ac.uk/surf/guides/yag/iguide_top.html*.

Brennan S. and Cowan, P. L.: 1992, *Rev. Sci. Instrum.* **63**(1), 850.

Chen, M. H.: 1986, *Atomic Data Nucl. Data Tables* **34**, 301.

Culhane, J. L., *et al.*: 1991, *Solar Phys.* **136**, 89.

Dejus, R. J. and del Rio, M. S.: 1996, *Rev. Sci. Instrument.* **67(9)**. (http://www.esrf.fr/computing/scientific/xop/).

Dennis, B. R.: 2004, *private communication*.

Dubau, J.: 2004, *private communication*.

Feldman, U. and Laming, M.: 2000, *Phys. Scripta* **61**, 222.

Fludra, A. and Schmelz, J. T.: 1999, *Astron. Astrophys.* **348**, 286.

Kępa, A. and Sylwester, J.: 2005, *Astron. Astrophys.*, in preparation.

Kowalinski, M. and Sylwester. J.: 2004, *Internal Report*, RESIN Data Reduction Package for RESIK.

Kowalinski, M., Kordylewski, Z., Sylwester. J., Trzebinski, W., and Lisin, D.: 2004, *Proceedings: IAU Symposium* **223**, submitted for publication.

Lapington, J., Culhane, J. L., Trow, M. W., and Bentley, R. D.: 1990, *Proc. SPIE* **1159**, 252.

Lebedev, N. I., Oraevsky, V. N., and Zhugzda, Y. D.: 1995, *Astron. Astrophys.* **296**, L25.

Lin, R. P., *et al.*: 2002, *Solar Phys.* **210**, 3.

Lugovskaya, O. M. and Stepanov, S. A.: 1991, *Sov. Phys. Crystallogr.* **36**, 478. (http://sergey.gmca.aps.anl.gov/x0h.html).

Meyer, J.-P.: 1985, *Astrophys. J. Suppl.* **57**, 173.

Oda, M., Muranaka, N., Matsuoka, M., Miyamoto, S., and Ogawara, Y.: 1976, *Space Sci. Instrum.* **2**, 141.

Oraevsky, V. N. and Sobelman, I. I.: 2002, *Astron. Lett.* **28**, 401.

Phillips, A.: 1994, *private communication*.

Phillips, K. J. H., Sylwester, J., Sylwester, B., and Landi, E.: 2003, *ApJ* **589**, L113.

Phillips, K. J. H., Dubau, J. Sylwester, B., Sylwester, J., Culhane, J. L., Doschek, G. A., and Lang, J.: 2004, *Adv. Space Res.*, in press.

Pradhan, A.: 1985, *Astrophys. J. Suppl.* **59**, 183.

RESIK Weekly Newsletters: 2003, in B. Sylwester and J. Sylwester (eds.), *http://www.cbk.pan.wroc.pl/weekly_archive/szablon.htm*.

Rapley, C. G., Culhane, J. L., Acton, L. W., Catura, R. C., Joki, E. G., and Bakke, J. C.: 1977, *Rev. Sci. Instrum.* **48**, 1123.

Sylwester, J., Lemen, J. R., and Mewe, R.: 1984, *Nature* **310**, 665.
Sylwester, J., Culhane, J. L., Doschek, G. A., Oraevsky, V. N., Phillips, K. J. H., and Sylwester, B.: 2002, in *Proceedings of the Tenth European Solar Physics Meeting*, September 2002, Prague, Czech Republic, ESA SP-506, p. 765.
Sylwester, J., Sylwester, B., Culhane, J. L., Doschek, G. A., Oraevsky, V. N., and Phillips, K. J. H.: 2003, in *Proceedings of the ISCS 2003 Symposium, "Solar Variability as an Input to the Earth's Environment"*, Tatranská Lomnica, Slovakia, ESA SP-535, p. 733.
Sylwester, J., Kowalinski, M., Sylwester, B., and Bąkała, J.: 2004a, *manuscript in preparation*.
Sylwester, J., Sylwester, B, Kowalinski, M., and Bąkała, J.: 2004b, *manuscript in preparation*.
Trow, M., Bento, A. C. and Smith, A.: 1994, *Nucl. Instrum. Methods* **348**, 232.
Young, P. R., Del Zanna, G., Landi, E., Dere, K. P., Mason, H. E., and Landini, M.: 2003, *Astrophys. J. Suppl.* **144**, 135, *CHIANTI*.